Two-layer Hall effect model for intermediate band Ti-implanted silicon

J. Olea, G. González-Díaz, D. Pastor, I. Mártil, A. Martí, E. Antolín, and A. Luque

Citation: Journal of Applied Physics **109**, 063718 (2011); doi: 10.1063/1.3561374
View online: http://dx.doi.org/10.1063/1.3561374
View Table of Contents: http://scitation.aip.org/content/aip/journal/jap/109/6?ver=pdfcov
Published by the AIP Publishing

Two-layer Hall effect model for intermediate band Ti-implanted silicon

J. Olea,[1,a)] G. González-Díaz,[1] D. Pastor,[1] I. Mártil,[1] A. Martí,[2] E. Antolín,[2] and A. Luque[2]
[1]*Departamento de Física Aplicada III (Electricidad y Electrónica), Facultad de Ciencias Físicas, Universidad Complutense de Madrid, Av. Complutense s/n, Ciudad Universitaria, 28040 Madrid, Spain*
[2]*Instituto de Energía Solar, Escuela Técnica Superior de Ingenieros de Telecomunicación, Universidad Politécnica de Madrid, Av. Complutense s/n, Ciudad Universitaria, 28040 Madrid, Spain*

(Received 3 November 2010; accepted 3 February 2011; published online 24 March 2011)

Si samples have been implanted with very high Ti doses (over the theoretical Mott limit) to obtain an intermediate band (IB) in the host semiconductor. The electronic transport properties of this material have been analyzed by temperature-dependent sheet resistance and Hall effect measurements in the 7–400 K range. The experimental results are successfully explained by means of an analytical two-layer model, in which the implanted layer and the substrate behave as an IB/n-Si type junction. We deduce that the IB is located at 0.38 eV below the conduction band, which is around one third of the Si bandgap, i.e., theoretically close to the optimum location for an IB. Finally, we obtain that carriers at the IB behave as holes with a mobility of 0.4–0.6 $cm^2\ V^{-1}\ s^{-1}$. This extremely low mobility is the one expected for a semifilled, metallic band, being this metallic condition of the IB a requirement for IB solar cells. © *2011 American Institute of Physics*. [doi:10.1063/1.3561374]

I. INTRODUCTION

The intermediate band (IB) solar cell has been proposed as a candidate for the third generation of photovoltaics.[1] Following IB theory, the IB can be obtained in standard semiconductors by the introduction of deep levels in concentration above the Mott transition limit.[2] A semiconductor with an IB (IBS) behaves like a "three" band semiconductor [valence band, conduction band (CB) and an IB located within the otherwise conventional bandgap]. One of the main consequences of this fact is that, under nonequilibrium conditions, this semiconductor has three quasi-Fermi levels.

The formation of an IB by ion implantation is a difficult task because it involves massive impurifying of the semiconductor host plus postimplantation techniques such as nonequilibrium annealing. We have used ion implantation and laser annealing[3] to modify a thin layer on the silicon surface avoiding the formation of secondary phases. Consequently, in order to analyze the transport properties of an IBS, we have to deal with a two-layer heterogeneous system, formed by the implanted layer and by the unimplanted substrate.

Different two-layer models have been recently proposed to understand Hall effect measurements of different compound semiconductors in which an unintentional two-layer behavior has been observed, shadowing the bulk electrical behavior: ZnO (surface conductive layer)[4] and GaN (semiconductor/substrate interface degenerated layer).[5]

In principle, Si would not be the most suitable semiconductor to be used as host semiconductor to build IB solar cells, due to its relatively low bandgap value, as it has been recently reported by some of us,[6] because the detailed balance limiting the efficiency of a IB solar cell with a bandgap value below 1.14 eV is very close than that of the conventional single junction cell counterpart. However, when no-idealities such as nonradiative recombination are taken into account, as pointed out in Ref. 6, there should be room for improvement by introducing an IB material in practical devices. Moreover, some authors point out that the potential efficiency for IB Si solar cell would be very high.[7] Nevertheless, Si-based solar cells cover more than 90% of the market, and thus any increase in the efficiency of Si solar cells, even low, would be of extremely importance. Moreover, as Si is a well-known semiconductor, any knowledge on the IB field learned from the Si-based research may be applicable to other IB materials. As a consequence, practical realization of the IB concept in this semiconductor would give a better understanding of physical principles involved in the IB solar cell operation.

In two recent papers, we have shown that Ti-implanted Si above Mott limit forms an IBS.[8,9] In Ref. 8 we have highlighted an important aspect: the rectifying character of the IBS/n-Si substrate junction at low temperatures. On the other hand, in Ref. 9, we have successfully fitted the measured sheet resistance of samples with the ATLAS code.[10] However, as this code could not simulate an IBS, we artificially introduced in the ATLAS framework a pseudosemiconductor in which the valence band emulated the IB, with an almost constant hole density, and the CB was similar to the Si one. In this modeling, the semiconductor gap became just the difference between the IB and the CB. This model has proven to work fine calculating the sheet resistance but fails when attempting to fit the Hall mobility results because of convergence problems. Additionally, the introduction in the ATLAS code of a pseudosemiconductor is a cause of concern.

A key question is to elucidate the physical origin of the IBS. Rutherford backscattering measurements showed that the Ti atoms within the Si lattice are located mostly interstitially.[9] P. Wahnón and co-workers[11] have recently shown through

[a)]Author to whom correspondence should be addressed. Electronic mail: oleaariza@fis.ucm.es.

ab initio calculations that the Ti interstitial atoms in a host Si lattice could produce an IBS. As the Ti electronic configuration is $1s^2 2s^2 2p^6 3s^2 3p^6 4s^2 3d^2$, each atom is able to give one to four electrons to the IB.

In this paper we propose for the first time in our knowledge an analytical two-layer model based on van der Pauw's one to explain satisfactorily both sheet resistance and Hall effect measurements of Ti-implanted Si IBS. The main difference between the model presented here and those previously reported[8,9] is the consideration of the current limitation between the implanted layer and the substrate introduced by the rectifying behavior of the implanted–substrate junction. The details dealing with this junction were previously reported in Ref. 8.

II. EXPERIMENTAL

Single crystal n-Si samples ($\rho = 200\ \Omega\cdot$cm; $\mu = 1450$ cm^2/Vs; $n = 2.2 \times 10^{13}$ cm^{-3} measured at 300 K) were implanted with Ti ions by means of a VARIAN CF3000 Ion Implanter refurbished by Ion Beam Services (France). Ti was implanted at 30 keV with three different doses: 10^{15}, 5×10^{15}, and 10^{16} cm^{-2}. Then, the implanted Si samples were annealed by means of the pulsed laser melting (PLM) method[12] to recover the crystal lattice. The combination of two highly nonequilibrium techniques (ion implantation and subsequent PLM treatment) allows us to buildup a new class of semiconductors that avoid equilibrium constraints.[13] The PLM annealing process was performed by J. P. Sercel Associates Inc. (New Hampshire, USA). Samples were annealed with one 20 ns long pulse of a KrF excimer laser (248 nm) at energy density of 0.6–0.8 J/cm^2. PLM is a highly nonequilibrium processing technique which is able to melt and recrystallize the Si surface up to about tens of nanometer deep in very short times (10^{-8}–10^{-6} s). This rapid recrystallization time allows the incorporation of Ti atoms to the Si at concentrations well above the solubility limit for this element.[14] Also, the PLM processing of the Ti-implanted Si layer prevents secondary phase formation (i.e., Ti silicide) even when the equilibrium solubility limit has been greatly exceeded.[15]

Si-implanted samples were electrically characterized by sheet resistance and Hall effect measurements with the van der Pauw configuration at variable temperature using a Keithley SCS 4200 model with four source and measure units. Samples were 1×1 cm^2 pieces of 300 μm thick Si wafers with four Al electrodes in the corners. Electrodes were triangular shaped with about 1.5 mm cathetus. The magnetic field was 1 T. The samples were placed inside a homemade liquid nitrogen cryostat attached to a vacuum pump to avoid moisture condensation. The temperature was varied between 90 and 380 K. We measured the four van der Pauw configurations and also changed the polarity of current source and the direction of the magnetic field to minimize the spurious thermo-galvanomagnetic effects. In some samples, measurements were extended down to 7 K with a closed cycle Janis cryostat.

Lifetime measurements of the samples have been reported elsewhere.[16]

III. RESULTS

Figures 1 and 2 show the sheet resistance and Hall mobility, respectively, as a function of the absolute temperature (90–380 K) for the three different implantation doses and a nonimplanted substrate that will act as reference. The figures also include the fitting curves resulting from the model that will be described in Sec. IV of this paper. Figure 1 shows that the sheet resistance for implanted samples and for low temperatures is higher than the substrate sheet resistance. This is not consistent, since having two parallel layers, the sheet resistance of the whole structure should be lower than the sheet resistance of one of the layers.

Time-of-Flight secondary ion mass spectrometry (ToF-SIMS) measurements of the samples with the three analyzed doses showed that Mott limit was surpassed before and after the PLM treatment.[17] It has been predicted that the IB is only possible if the Ti volume concentration is over the Mott transition limit.[2] Theoretical calculations indicate that this limit is $N_{Mott} \approx 6 \times 10^{19}$ cm^{-3} for Si.

ToF-SIMS measurements after the annealing show that this limit is exceeded up to a sample thickness of 20, 50, and 80 nm for doses of 10^{15}, 5×10^{15}, and 10^{16} cm^{-2}, respectively. Assuming as a first approach that the implanted profile is rectangular, we obtain the Ti concentration of 3×10^{20} cm^{-3}, 5×10^{20} cm^{-3}, and 7.5×10^{20} cm^{-3} for the doses previously mentioned. The rectangular profile is a rather realistic assumption, since the PLM annealing produces very abrupt profiles. For this calculation we have taken into account losses of about 40% on the Ti concentration due to the push-out effect during the film regrowth after the PLM treatment.[9] These concentrations are well above the Mott limit and, as a consequence, delocalization of the impurity electron wavefunctions should take place and the IB should be formed in the Ti-implanted layer. Although the proposed values are over the Mott limit, the Ti concentration that would give the highest efficiency in an IB-Si device remains as an open question. To highlight this issue, further research

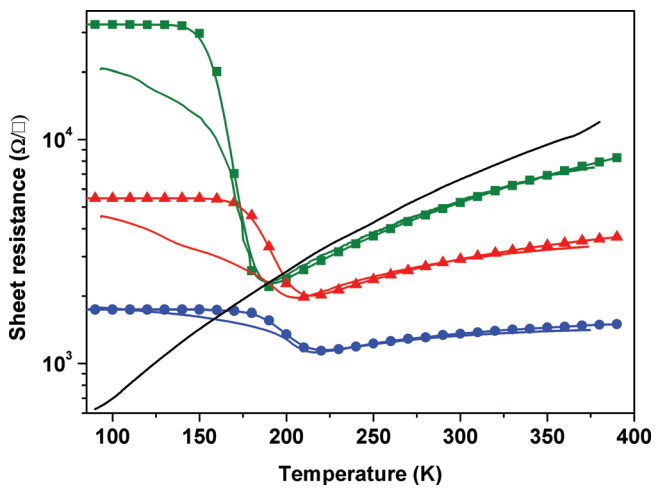

FIG. 1. (Color) Sheet resistance as a function of the measured temperature for different implantation doses: 10^{15} cm^{-2} (green); 5×10^{15} cm^{-2} (red); 10^{16} cm^{-2} (blue); and nonimplanted substrate (black). Model fitting of the sheet resistance for the three analyzed doses: 10^{15} cm^{-2} (■) 5×10^{15} cm^{-2} (▲) and 10^{16} cm^{-2} (●).

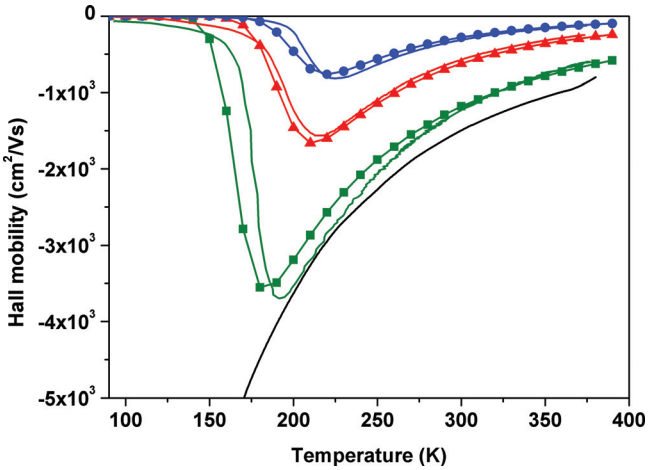

FIG. 2. (Color) Hall mobility for the same samples as in Fig. 1: 10^{15} cm^{-2} (green); 5×10^{15} cm^{-2} (red); 10^{16} cm^{-2} (blue); and nonimplanted substrate (black). Model fitting of the Hall mobility for the three analyzed doses: 10^{15} cm^{-2} (■) 5×10^{15} cm^{-2} (▲) and 10^{16} cm^{-2} (●).

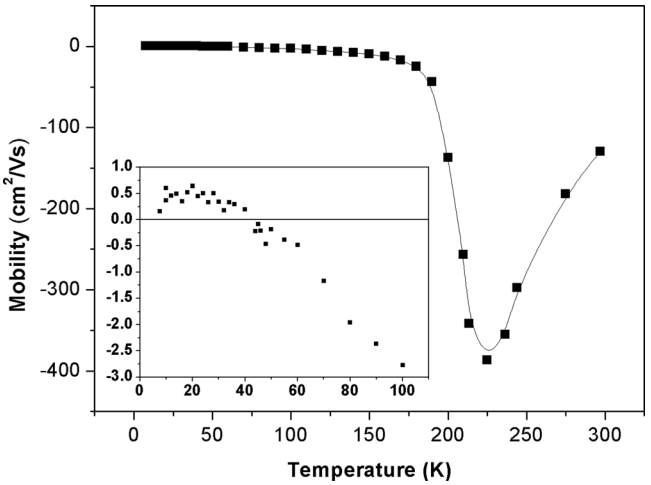

FIG. 4. Hall mobility for a sample implanted with 10^{16} cm^{-2} annealed at 0.8 J/cm^2 and measured down to 7 K. The inset shows the change from n- to p-type conduction when the temperature decreases.

on complete devices using Ti-implanted Si as IB material should be performed. In the following text, we will designate the implanted layer as the IBS.

Regarding Hall effect measurements shown in Fig. 2, it can be seen that, at low temperatures, the Hall mobility decreases as temperature goes down. The detail on how the measured Hall mobility behaves in the low temperature range is shown in Figs. 3 and 4 for two different samples. It is clearly seen in both samples that the bilayer Hall mobility changes its polarity from negative at high temperatures to positive at low temperatures. The different temperature at which the polarity change occurs is due to the different processing conditions of the samples and will be detailed in Sec. V.

In Ref. 9 we proposed for the IBS/n-Si junction the band diagram depicted in Fig. 5 of this paper. From a transport point of view, the electrons located at the IB could behave as electrons or holes depending on the concave or convex curvature of the E-k diagram and the degree of filling of the IB, accordingly to quantum-mechanical formulation.[11] According to the results in Figs. 3 and 4, at low temperatures, that is, when the transport properties are dominated by the IBS,[9] the Hall mobility polarity is always *p*-type and the carrier mobility at the IBS should be any case very low, also a consequence of the bandwidth.[18]

As predicted by the IBS theory,[19] the Fermi level should be pinned at the IB due to the high charge concentration at this energy, i.e., the IB is a "semimetallic" band. Any charge change could be neutralized by minimum Fermi level variation around the IB level. At the junction between the implanted layer and the substrate, the I–V characteristics should be determined by the electrons in both layers, having in mind that the holes at the IBS could not go to the substrate due to the lack of continuity of the IB (see Fig. 5), and that there are almost no holes in the substrate or in the valence band at the IBS.

At low temperature (90 K), the substrate Fermi level is located about 0.1 eV down the CB and, if the IB is deeper than this energy, there is a blocking barrier at the interface which controls the current from the implanted layer to the

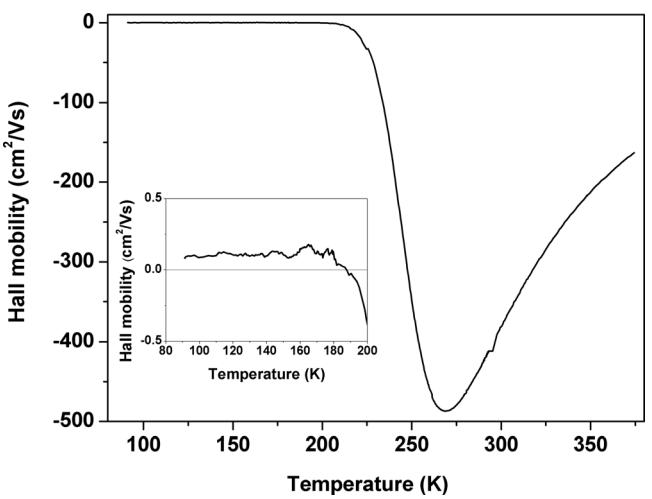

FIG. 3. Hall mobility for a sample implanted with a 5×10^{15} cm^{-2} dose and annealed at 0.6 J/cm^2. The inset shows the change from n to p-type conduction when the temperature decreases.

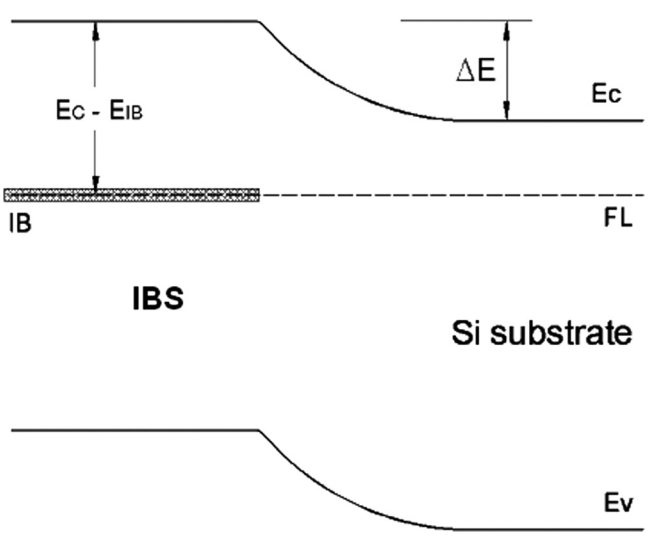

FIG. 5. Generic band diagram of the IBS/n-Si double sheet.

substrate. That behavior has been modeled in Ref. 8, proving that saturation current for this phenomenon has an exponential dependence with the difference between the CB energy and the IB energy (E_C–E_{IB}). This is therefore the main current limiting mechanism that produces the decoupling between the IBS and the substrate.[9] For the practical purposes of this paper, this limiting current will be modeled as a resistor as detailed in Sec. IV A.

IV. PROPOSED MODEL

A. Sheet resistance

For greater generality we will designate the IBS layer as layer 1 and the substrate as layer 2. Electron density at the CB of the IBS will be designated as n_1 and its mobility as μ_{n1}. Hole density at the IB will be designated as p_1 and its mobility as μ_{p1}. Substrate electron parameters are n_2 and μ_{n2}.

An electrical equivalent circuit for this bilayer structure is depicted in Fig. 6. We will assume that both layers are connected with four nonideal diodes (one on each corner) that represent the electrical IBS-substrate junction. This model is, strictly speaking, nonlinear but we will assume, as advanced before, that the limiting characteristics introduced by the nonideal diode can be modeled by a temperature depending resistor R_t when the diode is in inverse polarization:

$$R_t = \frac{1}{G_t} = A\exp(E_C - E_{IB})/kT. \tag{1}$$

This approximation can be done because, for the purpose of this work, the actual value of the resistor is not relevant but only its dependence with the temperature. Besides, as explained below, the preexponential factor A will be obtained as a fitting parameter. Direct polarized diodes will be modeled by short circuits.

Currents I_1 and I_2 at layers 1 and 2 can now be obtained as

$$\begin{aligned} I_1 &= V/R_{P1} \\ I_2 &= V/(R_t + R_{P2}) \end{aligned} \tag{2}$$

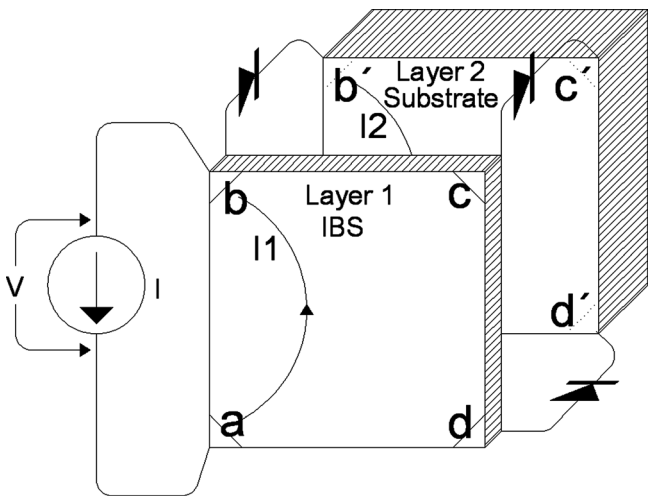

FIG. 6. Exploded view of the double layer showing current limiting diodes connecting the two layers.

where V is the voltage drop at the current source terminals. Obviously $I = I_1 + I_2$. R_{P1} and R_{P2} are the resistances between two consecutive electrodes (a and b in Fig. 6) for layer 1 and (a' and b') for layer 2. The relation between the sheet resistance R_s of a layer and the resistance seen from the electrodes R_p is not obvious. In the Appendix, we prove that can be written as $R_P = \alpha R_S$, depending only on the geometrical relation between the electrode size and the sample size. According to the Appendix, and taking into account the relative electrode size in our samples, the α factor should be approximately 2.

Rewriting expressions in Eq. (2), $I_1 = V/\alpha R_{S1}$ and $I_2 = V/(R_t + \alpha R_{S2})$. Due to the presence of the R_t, the developed voltage on the opposite corners (van der Pauw voltage corners) is not the same for both layers (it would the same only if the injected current on each layer is in a inverse proportion to the sheet resistance). To obtain the measured voltage we have to bear in mind the internal impedance across which the voltage is developed,[20] as represented in Fig. 7.

Each one of the voltages ΔV can be expressed according to van der Pauw as

$$\begin{aligned} \Delta V_1 &= I_1 \,.\, R_{S1} \,.\ln(2)/\pi \\ \Delta V_2 &= I_2 \,.\, R_{S2} \,.\ln(2)/\pi \end{aligned} \tag{3}$$

and the equivalent voltage measured on the electrodes of the top layer (electrodes d and c in Fig. 7) with an infinite impedance voltmeter would be

$$\Delta V = \Delta V_1 - R_{p1}\frac{\Delta V_1 - \Delta V_2}{(R_t + R_{p1} + R_{p2})} = \frac{\Delta V_1 G_{p1} + \Delta V_2 \dfrac{G_t G_{p2}}{G_t + G_{p2}}}{G_{p1} + \dfrac{G_t G_{p2}}{G_t + G_{p2}}}, \tag{4}$$

where G_{P1} and G_{P2} are the conductances of the IBS and the substrate, respectively, i.e., $G_{p1} = 1/R_{P1} = q(n_1\mu_{n1} + p_1\mu_{p1})\, t_1/\alpha$, $G_{p2} = 1/R_{P2} = q n_2 \mu_{n2}\, t_2/\alpha$ being t_1 the IBS thickness and t_2 the substrate thickness.

Equation (4) can be written in a more compact way if we introduce a function $F = G_t/(G_t + G_{p2})$

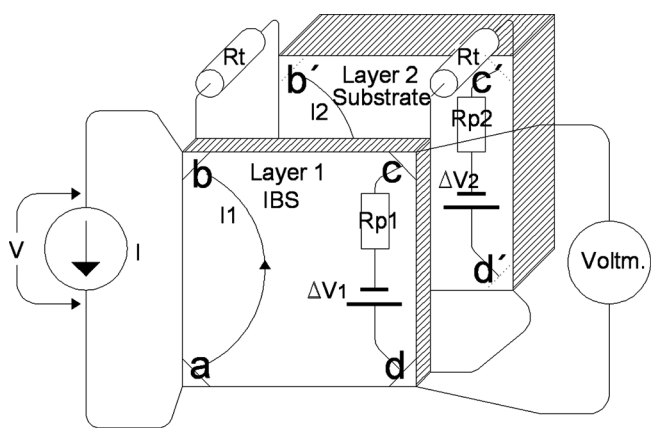

FIG. 7. Exploded view of the double layer showing the equivalent voltages at the potential corners and its internal resistances. Diodes have been replaced by short circuits or resistors depending on the direct or inverse polarization.

$$\Delta V = \frac{\Delta V_1 G_{p1} + \Delta V_2 G_{p2} F}{G_{p1} + G_{p2} F}. \quad (5)$$

The equivalent sheet resistance, R_{sheet}, i.e., the one measured on top of the layer 1 is

$$R_{\text{sheet}} = \frac{\pi}{\ln(2)} \frac{\Delta V}{I} = \frac{\pi}{\ln(2)} \frac{\Delta V}{\{V/R_{p1} + V/(R_t + R_{p2})\}} = \frac{G_{p1} + \frac{G_t^2 G_{p2}}{(G_t + G_{p2})^2}}{\left\{G_{p1} + \frac{G_t G_{p2}}{G_t + G_{p2}}\right\}^2}. \quad (6)$$

Introducing the function F in the sheet resistance formula we can write

$$R_{\text{sheet}} = \frac{G_{p1} + G_{p2} F^2}{\alpha (G_{p1} + G_{p2} F)^2}. \quad (7)$$

In Eqs. (6) and (7), R_{sheet} tends toward R_{S1} when G_t or F tends toward zero and (R_{sheet} tends) toward the value for R_{s1} in parallel with R_{s2} when G_t tends toward infinity and F tends toward 1.

B. Function *V/ΔV*

An important insight of the sample behavior could be obtained measuring not only the current injected to the electrodes but also the voltage V developed at the current source. It is easy to prove that $V/\Delta V$ for a simple layer is $\alpha\pi/\ln(2)$ whenever the contacts are ohmic and there is no appreciable voltage drop at them. Also, a two-layer that could be assumed to be electrically in parallel (i.e., with $R_t = 0$) has also the same value for $V/\Delta V$; in fact the voltage developed in both layers is the same since the injected current splits in portions which are inversely proportional to the sheet resistance.

In a more complex situation, as it is the one we have in our samples, $V/\Delta V$ can be written as

$$\frac{V}{\Delta V} = \frac{\alpha\pi}{\ln(2)} \frac{G_{p1} + \frac{G_t G_{p2}}{G_t + G_{p2}}}{G_{p1} + \frac{G_t^2 G_{p2}}{(G_t + G_{p2})^2}} = \frac{\alpha\pi}{\ln(2)} \frac{G_{p1} + G_{p2} F}{G_{p1} + G_{p2} F^2}. \quad (8)$$

As it can be seen, $V/\Delta V$ goes to $\alpha\pi/\ln(2)$ whenever G_t tends toward 0 or infinity (F toward 0 or toward 1).

C. Hall mobility

A similar procedure can be used to find the effective Hall mobility

$$\mu_{\text{eff}} = \frac{-\mu_{n1} G_{pe1} + \mu_{h1} G_{ph1} - \mu_{n2} G_t G_{p2}/G_t + G_{p2}}{G_{pe1} + G_{ph1} + G_t G_{p2}/G_t + G_{p2}} = \frac{-\mu_{n1} G_{pe1} + \mu_{h1} G_{ph1} - \mu_{n2} G_{p2} F}{G_{pe1} + G_{ph1} + G_{p2} F}, \quad (9)$$

where G_{Pe1} is the electron conductance due to the electrons on the implanted layer CB ($G_{pe1} = q n_1 \mu_{n1} t_1/\alpha$), G_{ph1} is the hole conductance due to the holes at the IB ($G_{ph1} = q p_1 \mu_{p1} t_1/\alpha$) being G_{p2} and G_t the same as the ones defined in Sec. IV A.

Now the α coefficient has to be changed from 2 to 2.2 which is the correct value for R_p/R_s when the current is injected at the opposed electrodes in a square sample with relative electrode size as the ones that characterize our samples. This is explained in the Appendix.

Equation (9) shows clearly the meaning of the F function. At low temperatures F goes to 0 and the measured mobility is just the implanted layer mobility while at high temperature F goes to 1 and we have the compound mobility between the layer and the substrate. Consequently, the F function is the "decoupling" function responsible of the independence of the implanted layer at low temperatures.

V. COMPARISON BETWEEN THE MODEL AND THE EXPERIMENTAL RESULTS

In order to simulate the two-layer behavior and to compare with the experimental results, some parameters have to be chosen.

1. Hole concentration in the IB (p_1) and mobility (μ_p): Assuming the implanted Ti concentration remaining in the sample after laser annealing is located interstitially, we will have a carrier density from 1 to 4 times this concentration. The mobility should be very low as corresponding with an IB.[21] Best fits are obtained with mobilities between 0.4 and 0.6 cm^2/Vs, which correspond to the mobilities obtained experimentally. We will assume that the carriers behave like holes, being consequently its mobility positive.

2. Electron concentration in the IBS layer (n_1) and mobility (μ_{n1}): The concentration is determined by the IB position trough Maxwell Boltzmann statistics $n_1 = N_c \exp(E_C - E_{IB})/kT$. It is supposed that the IB has so many electrons that their promotion to the CB does not change its density. Mobility at this band has to be reduced in comparison to the substrate mobility, since the high Ti-implanted dose produces a certain amount of lattice alteration. As the IB hole concentration times the hole mobility is higher than the electron concentration times the electron mobility for all the temperatures, these parameters does not affect the fitting.

3. Electron concentration at the substrate (n_2) and mobility (μ_{n2}): Their value has been previously measured finding a temperature independent electron concentration of $2.2 \times 10^{13}\ \text{cm}^{-3}$ and a mobility that could be fitted to 1450 $(T/300)^{-2.2}\ \text{cm}^2/\text{Vs}$.

In order to fit the model to the experimental measurements we have, therefore, to scan just three parameters: the IB energy (we assume is the same for all the samples), hole mobility at the IB, and the A parameter of the diode saturation current. All the other parameters are determined by direct measurements (IBS thickness) or are a consequence of the model (hole concentration at the IB).

Figures 1 and 2 show a comparison between our model and the experimental sheet resistance and mobility data. Both are fitted using the parameters quoted in Table I. The IB energetic position deduced from this analysis is 0.38 eV below the CB. This location should be close to the optimum since as a rule of thumb, the optimum position for the IB is

TABLE I. Best fitting figures for the three doses analyzed (rows). First column gives the energy position of the IB, second one pre-exponential factor for the transversal resistance R_t, and the third one the hole mobility at the IB.

Dose (cm^{-2})	E_C-E_{IB} (eV)	A (A)	μ_{pc} (cm^2/Vs)
10^{15}	0.38	2×10^{-7}	0.4
5×10^{15}	0.38	3×10^{-6}	0.4
10^{16}	0.38	5×10^{-6}	0.6

about one third of the host semiconductor bandgap below the CB or over the valence band.[1] On the other hand, the measured values for the carrier mobility at the IB are extremely low, suggesting that the IB is a metallic, semifilled-band. This semifilled-band is the optimum configuration for a high efficiency device since a filled or empty band would not allow one of the sub-bandgap transitions. The low mobility values should not affect negatively the efficiency of the final device as in a IB solar cell, the IB has to be isolated from the other bands and thus conduction in the IB would not be necessary. Moreover, the IB would act as an "energy step" to promote the absorption of photons with energy lower than the bandgap by means of a two-step transition and thus the IB does not play any role in the carrier collection process.

In Fig. 1, the temperature at the resistance notch (about 180 K for 10^{15} cm^{-2} dose) marks the border between decoupled layers at the left of the plot or coupled ones for higher temperatures. At lower temperatures, the R_t resistance is high enough so that only the IBS layer is measured. For higher temperatures we observe both layers in parallel.

According to the previous explanation, the plateau at temperatures below the notch in Fig. 1 should be due just to the IBS layer, i.e., to the holes at the IB and electrons at the CB. The latter ones are negligible according to Maxwell Boltzmann statistics for an IB energetic position of 0.38 eV. Consequently this sheet resistance is $1/q\mu_{p1}p_1t_1$. This plateau is reached quicker in the model than in the experimental results probably due to some leakage currents through the sample perimeter which is a strongly damaged zone. When the van der Pauw setup is polarized, the junction below one of the contact (see Fig. 6 for sake of clarity) is inverse polarized, and an important path for carriers could be formed in the sample rims that would affect the transport properties of the sample.

As the previously defined plateau at low temperatures is a function of p_1 times μ_{p1}, we cannot really know the hole concentration nor the hole mobility. We can only guarantee the product of both quantities. In this respect we must assume an uncertainty of 1–4 times in the hole concentration and in the hole mobility at the IB.

The temperature for the resistance minimum is strongly dependent on the IB energy position and less dependent on the A parameter. Above this temperature the sheet resistance depends on all the parameters quoted in Sec. IV A.

Figure 8 plots the $V/\Delta V$ factor for the sample implanted with a 10^{15} cm^{-2} dose. As explained before, the value of this function should be $\alpha\pi/\ln(2)$ whenever the sample is just a simple layer or when the bilayer is effectively in parallel (R_t negligible in comparison with R_{p2}). For a geometrical factor

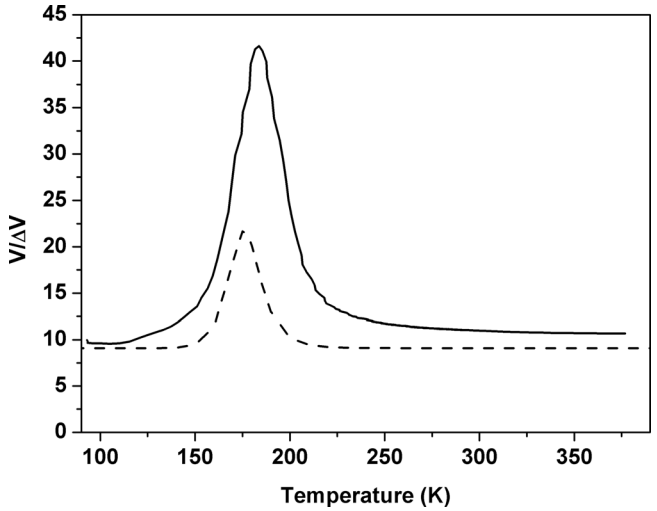

FIG. 8. $V/\Delta V$ function for the sample with 10^{15} cm^{-2} dose (solid line: experimental; dotted line: model).

$\alpha=2$ (meaning each electrode is about 1/6 of the sample side), $V/\Delta V$ should be 9, very close to the experimental value both for low and for high temperature. For intermediate temperatures the $V/\Delta V$ function has a maximum, as predicted by Eq. (8). The similitude between the theoretical value and the experimental one certifies that the contacts to the IBS layer are ohmic, otherwise the experimental value would have been much higher than the theoretical one. The measurement of $V/\Delta V$ is an easy method to know the contact resistance mainly if there are no possibilities to make transversal measurements.

The decoupling function F is represented in Fig. 9 for the three doses analyzed. The function is very similar irrespective of the doses except for a slight temperature displacement.

One of the most interesting aspects of this work is the nature of the carriers at the IB. The model here proposed for the bilayer behavior is independent of this nature and it is only dependent on the barrier current limitation for the electrons. Consequently, the model would work for both types of

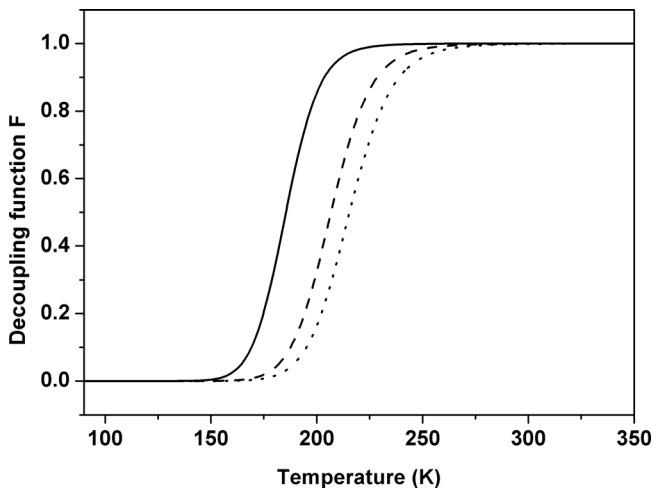

FIG. 9. The decoupling function represented vs the temperature for 10^{15} cm^{-2} dose (solid line), 5×10^{15} cm^{-2} (dashed line), and 1×10^{16} cm^{-2} (dotted line).

carriers at the IB. The impossibility of the IB carriers to go to the substrate is irrespective whether they are electrons or holes. The only difference we can find between electrons or holes is the change on the mobility sign, which would give us the type of the carriers at the IB. According to Figs. 2–4, the mobility decreases very quickly and an apparent change from n-type to p-type appears, at temperatures that depend on the sample processing conditions.

As predicted by the model, at low temperatures we are measuring only the IBS mobility:

$$\mu_{\text{eff}} = \frac{-\mu_{1e}G_{p1e} + \mu_{1h}G_{p1h}}{G_{p1e} + G_{p1h}}. \tag{10}$$

Samples with low electron mobility should change the polarity at higher temperatures, while in samples with higher electron mobility, the polarity change should be observed at lower temperatures. Figure 3 shows the Hall mobility of a sample implanted with a dose of 5×10^{15} cm^{-2} and annealed at 0.6 J/cm^2. This sample has presumably lower electron mobility because it has been annealed at a lower energy. The clear change on the polarity is shown in the inset of Fig. 3. The change is seen at $T = 190$ K. In Fig. 4 we plot the Hall mobility of a sample implanted with a 10^{16} cm^{-2} dose and PLM annealed at 0.8 J/cm^2. In this sample, the electron mobility should be higher because of the higher annealing energy density. Hall measurements were conducted down to a temperature of 7 K. The polarity change is also clearly evidenced at $T = 40$ K. Results in Figs. 3 and 4 are in full agreement with the prediction of Eq. (10).

VI. CONCLUSIONS

High dose Ti-implanted Si crystals show uncommon electrical characteristics that have been explained using the theory of IBS and a new model for the electrical conduction on a two-layer, heterogeneous system. The model takes into account the current limitation between the implanted layer and the substrate that was predicted by the IB theory. The electrical model shown here allows us to explain the coupling and decoupling characteristics of the two-layer and also to determine that there is no any impact of the electrical contacts, as they behave as ohmic ones.

Sheet resistance and mobility could be fitted just with three variables: the IB energy, the hole mobility at the IBS, and the pre-exponential factor of the junction saturation current. The IB energetic position is the same irrespective of the dose and the hole mobility is almost constant within the experimental errors. The energetic position of the IB is the same as the one determined in a previous work where this energy was determined using a simulation program.

The energy location of the IB deduced from the model proposed in this study is 0.38 eV below the CB, i.e., about one third of Si bandgap. This position should be close to the optimum for an IB in Si. Finally, the extremely low values obtained for the mobility of the carriers at the IB are typical of a metallic semifilled-band, and should not affect negatively the conversion efficiency of the final device.

ACKNOWLEDGMENTS

The authors would like to acknowledge C. A. I. de Técnicas Físicas of the Universidad Complutense de Madrid for ion implantation experiments. This work was partially supported by the Projects NUMANCIA-2 (S/2009/ENE-1477) funded by the Comunidad de Madrid and GENESIS-FV (CSD2006-00004) funded by the Spanish Consolider National Program and by the Grants (CCG07-UCM/TIC-2804), and (GR58/08) funded by U.C.M.-C.A.M.-B.S.C.H.

APPENDIX: RELATION α BETWEEN R_S AND R_P

We have to find the relations α between the resistance at the consecutive corners of a square layer (R_P) and the sheet resistance (R_S) of the same layer. Obviously, the resistance has a strong dependence on the contact shape and its size relative to the sample size. Assuming triangular contacts we will introduce the fraction between the contact side to the sample side as a parameter.

The resistance R_p has to be calculated numerically as there is no analytical model for it. We will model the layer as an array of resistors with 19 rows and 19 columns and we will use the popular PSPICE code[22] to find the α parameter quoted above. Resistors at the borders should have twice value because there is not current path outside these limits.[23] For easy calculation we will use 1 Ω resistor and we will inject a 1 A current between two consecutive contacts and we will register the potential on the current source (V) and potentials at the opposite corners (V_a and V_b) for different contact size. In Table II we collect the results of this simulation.

Column 1 is the contact size, i.e., the number of nodes that have been short circuited at the corners to simulate the equipotential triangular contact. The relative size could be obtained having in mind that the mesh size is 19×19. The second one is the differential voltage at potential measurement corners, the third one is the sheet resistance obtained with the classical van der Pauw formula $Rs = \pi/ln(2)\ \Delta V/I$. It is important to realize that the sheet resistance is just the resistance of each one of the differential elements we used to represent the complete sample. The α factor is simply the voltage developed at the current source because the current is 1 A and the sheet resistance is 1 Ω.

TABLE II. Simulation results from a 19×19 1 Ω resistor mesh with variable size triangular contacts. Columns are the contact size, the measured differential voltage at potential corners, the sheet resistance deduced form the van der Paw formula, the α factor, the $V/\Delta V$ function, and the error in the sheet resistance.

Contact size	ΔV	R_s	α factor	$V/\Delta V$	Error (%)
1×1	0.222	1.006	5.174	23.306	0.610
2×2	0.222	1.004	2.390	10.785	0.429
3×3	0.220	0.999	1.901	8.623	−0.115
4×4	0.217	0.983	1.542	7.114	−1.746
5×5	0.210	0.951	1.255	5.981	−4.919

TABLE III. α factor for a square layer simulated with a 19×19 mesh when the contacts are at opposite sample sides.

Contact size	α factor
1×1	5.394
2×2	2.610
3×3	2.140
4×4	1.711

For our sample, which has approximately 1.5 mm side triangular contacts, the α factor is very close to 2 and the $V/\Delta V$ figure is very close to 9. The error in the sheet resistance measurement is as low as 0.1%. Table III gives the same factor α when the electrodes are not consecutive but opposite.

[1]A. Luque and A. Martí, Phys. Rev. Lett. **78**, 5014 (1997).
[2]A. Luque, A. Martí, E. Antolín, and C. Tablero, Physica B **382**, 320 (2006).
[3]K. M. Yu, W. Walukiewicz, O. D. Dubon, J. Jasinski, Z. Liliental-Weber, J. Wu, J. W. Beeman, M. R. Pillai, and M. J. Aziz, J. Appl. Phys. **94**, 1043 (2003).
[4]D. C. Look, J. Appl. Phys. **104**, 063718 (2008).
[5]D. C. Look, D. C. Reynolds, J. W. Hemsky, J. R. Sizelove, R. L. Jones, and R. J. Molnar, Phys. Rev. Lett. **79**, 2273 (1997).
[6]A. Martí, D. Fuertes Marrón, and A. Luque, J. Appl. Phys. **103**, 073706 (2008).
[7]M. Ley, J. Boudaden, and Z. T. Kuznicki, J. Appl. Phys. **98**, 044905 (2005).
[8]G. Gonzalez-Díaz, J. Olea, I.Mártil, D. Pastor, A. Martí, E. Antolín, and A Luque, Sol. Energy Mater. Sol. Cells **93**, 1668 (2009).
[9]J. Olea, G. González Díaz, D. Pastor, and I. Mártil, J. Phys. D: Appl. Phys. **42**, 085110 (2009).
[10]ATLAS, Device Simulator Framewok distributed by Silvaco Data Systems Inc., 4701, Patrick Henry Drive, Bldg#6, Santa Clara, CA 95054 (2008).
[11]K. Sánchez, I. Aguilera, P. Palacios, and P. Wahnón, Phys. Rev. B **79**, 165203 (2009).
[12]C. W. White, S. R. Wilson, B. R. Appleton, and F. W. Young, Jr., J. Appl. Phys. **51**, 738 (1980).
[13]C. W. White, J. Narayan, and R. T. Young, Science **204**, 461 (1979).
[14]D. Mathiot and D. Barbier, J. Appl. Phys. **69**, 3878 (1991).
[15]J. Olea, M. Toledano-Luque, D. Pastor, G. González-Díaz, and I. Mártil, J. Appl. Phys. **104**, 016105 (2008).
[16]E. Antolín, A. Martí, J. Olea, D. Pastor, G. González-Díaz, I. Mártil, and A. Luque, Appl. Phys. Lett. **94**, 042115 (2009).
[17]J. Olea, M. Toledano-Luque, D. Pastor, E. San-Andrés, I. Mártil, and G. González-Díaz, J. Appl. Phys. **107**, 103524 (2010).
[18]S. Liu, K. Karrai, F. Dunmore, H. D. Drew, R. Wilson, and G. A. Thomas, Phys. Rev. B **48**, 11394 (1993).
[19]L. Cuadra, A. Martí, and A. Luque, Thin Solid Films 451–452, 593 (2004).
[20]R. L. Petritz, Phys. Rev. **110**, 1254 (1958).
[21]A. Aldea, Phys. Status Solidi (b) **22**, 377 (1967).
[22]PSPICE, Cadence Design Systems Inc., 2655 Seely Avenue, San Jose, CA 95134 (2000).
[23]D.W. Koon, Rev. Sci. Instrum. **77**, 094703 (2006).